BEHAVIOR OF FRP-STRENGTHENED RC ELEMENTS SUBJECTED TO PURE SHEAR

Mehdi Zomorodian[1], Guang Yang [2], Abdeldjelil Belarbi[3*], Ph.D., P.E., Ashraf Ayoub[4]

[1]Structural Engineer, Matrix Structural Engineers, Houston, USA. E-mail: mzomorodian@matrixstructural.com

[2]Graduate Engineer, Walter P Moore and Associates, Houston, USA. E-mail: gyang@walterpmoore.com

[3*]Hugh Roy and Lillie Cranz Cullen Distinguished Professor, Department of Civil and Environmental Engineering, University of Houston, Houston, USA. E-mail: belarbi@uh.edu

[4]Professor, City, University of London. E-mail: Ashraf.Ayoub.1@city.ac.uk

ABSTRACT

The shear behavior of fiber reinforced polymer strengthened reinforce concrete (FRP strengthened RC) has been the focus of extensive research studies. However, the mechanism of this complex phenomenon has not been fully clarified. Recent analytical models which were developed for predicting the shear capacity of FRP strengthened RC girders were based on test results of simply supported beam specimens with various shear span-to-depth ratios. In such tests no region of the specimen is subjected to uniform stress conditions, Therefore, the results of such tests cannot predict the true pure shear behavior due to non-uniformity of stresses, the presence of flexural and other non-shear related effects such as a/d ratio that cannot be filtered out. Therefore, proper design of shear strengthening using FRP requires testing of elements that are subjected to pure shear case primary before adding other governing effects. This allows a careful investigation and full understanding of the behavior at the element level. In order to accomplish this task, panel testing of representative RC specimens strengthened with FRP sheets were needed. This paper reports the testing of 10 FRP strengthened RC panels subjected to pure shear stress field. The tests were carried out to evaluate the effects of three

variables: FRP stiffness, FRP wrapping scheme, and transverse steel reinforcement ratio. The test results showed that these three variables greatly affected the shear behavior due to various types of failure modes associated with FRP strengthening. In addition, it was observed that the magnitude of increased shear capacity associated with the application of FRP sheets depends not only upon the stiffness of FRP, but also on the stiffness of internal shear reinforcement. With the increase of internal steel shear reinforcement, the effectiveness of shear gain due to externally bonded FRP decreases.

Keywords: Shear behavior; FRP strengthened RC members; Failure modes; Wrapping Scheme

INTRODUCTION

As a response to corrosion problems in reinforcing steel, and to increase the efficiency of strengthening systems in terms of time and ease of application, FRP composites have been increasingly used in rehabilitation and strengthening of RC structures [1]. The complex behavior of FRP-strengthened RC structures with predominant shear behavior has been previously studied through extensive experimental and analytical investigations [2-4]. Research related to the flexural behavior of FRP-strengthened elements has reached an advanced stage, and well established analytical models are available for analyzing and designing FRP-strengthened beams and columns under flexural and axial-confinement actions [1, 5]. However, the experimental and analytical research related to FRP strengthened RC under shear load are limited and has not been fully developed [6-10]

To predict the behavior of FRP-strengthened RC elements in shear, the truss model approach is commonly utilized by researchers [8, 11-12]. In the truss model analogy, constitutive laws of each component, namely concrete, steel, and FRP external reinforcement are crucial for

acceptable predictions. The results presented in this paper are part of a research work which aimed at developing a modified softening membrane model (SMM) for FRP-strengthened RC elements subjected to shear stress field. The SMM is based on a truss model and has been developed and was used to predict the entire shear stress-strain curve of the RC element under in-plane shear stress field [13]. The materials laws utilized is SMM was a work carried out by Belarbi et al. [14] and are widely accepted and used in several versions of the Softened truss models [13,15]. While adding external reinforcement such as FRP sheets, the behavior of elements such as concrete, steel and FRP are typically altered due to several effects such as the crack pattern, softened concrete struts, and Poison's ratio. The smeared stress-strain behavior of the constituents of strengthened member including concrete and reinforcing steel will be fundamentally different than their corresponding values for un-strengthened specimens. Consequently, different failure modes exist, and in turn affects the shear strength. In addition to the failure modes related to concrete in RC members such as diagonal tension failure in the web, shear compression failure in compression zone and flexure failure, FRP debonding and FRP rupture are common failure modes in FRP strengthened RC members [4, 11]. The problem is further complicated due to the presence of several additional parameters that might influence the behavior; parameters such as the properties of the FRP material, the angle of fiber direction, the characteristics of the fiber-resin interface and FRP-concrete interface, the presence of mechanical anchors, and the use of FRP strips as opposed to continuous sheets. These additional parameters modify the crack patterns, failure modes, and in turn influence the constitutive behavior of concrete [6,8,16]. Recent analytical models that were developed for predicting the shear capacity of FRP-strengthened RC beams are based on test results of simply supported beam specimens with various shear span-to-depth ratios. Results of

such tests cannot represent the true pure shear behavior due to the presence of flexural and other non-shear related effects that cannot be filtered out. As a result, a rational shear design cannot be accurately developed. An efficient method to evaluate the overall shear response of a member is to identify the characteristic behavior and the contribution of each element and material constituting the structure [17]. Reinforced concrete structures, such as shells and nuclear containment vessels, resist applied loads primarily through in-plane stresses. Each structure can be characterized as an assembly of elements, each subjected to two in-plane normal stresses and one in-plane shear stress [18]. To perform a rational analysis and thoroughly understand the behavior of FRP-strengthened RC structures, elements (panels) are isolated from the structure. Once a rational model is developed to predict the shear behavior in element level, the model can then be incorporated into a finite element program to predict the behavior of the whole structure.

The first step in the research was to experimentally investigate the shear constitutive behavior of FRP-strengthened RC elements subjected to pure shear. To evaluate such behavior, a series of full scale FRP-strengthened RC panels were constructed and tested using the Universal Panel Tester housed at the University of Houston [17]. Pure shear loading condition was simulated through proportionally applied biaxial tension-compression load. The test results of 10 elements (panels) subjected to pure shear loading are reported in this paper. The second step of the research was to develop an analytical model to predict the behavior of FRP-strengthened RC membrane elements subjected to pure shear. This new model, so-called the Softened Membrane Model for FRP-strengthened RC members (SMM-FRP), is described elsewhere [16,19].

The shear behavior of FRP-strengthened RC members is influenced by various factors. This study focuses on parameters that have been recognized by other researchers to have the most

95 influence on the behavior [6,8,20]. These parameters are (1) FRP reinforcement ratio (FRP
96 stiffness), (2) wrapping scheme, and (3) transverse steel reinforcement ratio.

97 **FRP Sheet Stiffness**

98 FRP sheet stiffness ($E_f t_f$)affects the contribution of FRP reinforcement to the overall
99 shear strength of FRP strengthened RC members. Previous research studies have indicated that
100 there exists a limit with respect to axial rigidity of the applied materials beyond which no
101 increase in shear capacity is expected [20]. When the thickness of the FRP sheets applied to RC
102 beam increases, the ultimate shear strength gain is limited by premature debonding from the
103 concrete substrate [21]. Also, the disproportionate strength gain when the FRP thickness (FRP
104 stiffness) increases is due to the fact that the ultimate failure is primarily governed by the
105 concrete cracking, splitting and loss of aggregate interlock [4]. Furthermore, as the FRP axial
106 stiffness increases, the effective strains in the sheets decrease [6], therefore, the FRP materials
107 will not reach their expected capacity before failure. In this case, the failure mode of the member
108 will be either concrete crushing or FRP debonding instead of FRP rupture.

109 Design guidelines such as ACI 440.2R-08 [1], CAN/CSA S806-12 [22] and *fib*-TG9.3 Bulletin
110 14 [23] fail to incorporate such behavior for strengthened beams when the thickness of FRP
111 sheets (and hence the stiffness) is high. These design guidelines are based on Triantafillou's [24]
112 statement that contribution to shear strength will increase with low values of axial stiffness.
113 Therefore, only when FRP sheets with low thickness is applied, the current design guidelines are
114 satisfactory [2].

115 **Wrapping Scheme**

The wrapping scheme affects the confinement due to the FRP sheets, and the potential for debonding. Common wrapping schemes in shear strengthening are fully wrap, side bond, U-Wrap, and U-wrap with FRP anchor.

The FRP anchor provides an effective way of anchoring the FRP composite to the RC substrate. There have been several studies regarding the design and implementation of FRP anchors [25-28]. The main parameters considered in designing the FRP anchors include the anchor diameter, number of anchors needed and anchor length. The FRP anchor used in this research had a diameter of 12.7 mm and a length of 610 mm as shown in Fig. 3. A contact length of 216 mm was used to cover the whole width of the FRP sheets with 6.5 mm extra on both sides, which satisfies the recommended length suggested by Kobayashi et al. [29].

Transverse Steel Reinforcement Ratio

Previous studies have revealed that the magnitude of increased shear capacity associated with the application of FRP materials depend not only upon the type of FRP that is being used, but also on the amount of internal shear reinforcement [8,21,30]. Researchers have indicated that the contribution of FRP in shear gain reduces when the beam is heavily reinforced in shear. This is because the maximum shear contributions of steel stirrups and FRP material may not be reached simultaneously. Also, with the increase of steel shear reinforcement, the measured effective strain reduces [6].

EXPERIMENTAL PROGRAM

In order to evaluate the shear behavior of FRP-strengthened RC members and to investigate the main factors that influence the behavior of such members, full-scale tests of 8 FRP-strengthened RC panels and 2 un-strengthened RC control panels were conducted.

The test panels were 1397×1397×178 mm (55×55×7 inches) in size, as shown in Fig. 1. The longitudinal and transverse steel reinforcements were arranged at a 45 degree angle with respect to the principal directions of the applied loads (1-2 coordinates) along *l* and *t* directions and the external FRP reinforcement was applied along transverse (*t*) direction. The steel reinforcement was grade 60 deformed bars with cross-sectional areas of 71 mm^2 (#3 rebar) and 129 mm^2 (#4 rebar) spaced at 188 mm in both longitudinal and transverse directions. The FRP sheets utilized in the experimental program which are typically used for shear strengthening in practice, consist of unidirectional carbon fibers attached on the two opposite surfaces of the panel specimens. The overall FRP sheet layout of the specimens is shown in Fig. 2a. The FRP strips had a width of 144 mm, and 188 mm center to center distance. The nominal strength of concrete was 52 MPa. The rebar was welded onto a pre-embedded connector inserts that were connected to the loading actuators by high-strength bolts. The steel reinforcement ratios and FRP sheet thicknesses were chosen carefully in order to study the effect of FRP stiffness on the shear behavior and also the effect of the ratio of FRP reinforcement to steel reinforcement. Three common wrapping schemes in shear strengthening are adopted, namely, 1) fully wrap, (2) side bond, and (3) U-wrap with FRP anchor. The fully wrap is to ensure that debonding is eliminated and the FRP will reach its ultimate strength, while the side bonding scheme is to evaluate the behavior up to FRP debonding occurs. The U-wrap with FRP anchor is to simulate the real case of shear strengthening with FRP in T-beams, where fully wrap method is infeasible due to the flanges. Fully wrap and side bonding wrapping scheme of the panels are shown in Fig. 2b and Fig.2c, respectively. Details of the U-wrap with FRP anchor are given in Fig. 3.

The test matrix in the experimental program is shown in Table 1. The specimens are identified using transverse rebar size (No.3 and 4), FRP thickness [0.6, 1 mm, and 2 mm (0.025, 0.040 and

161 0.080 inch)] and wrapping schemes, namely, Fully Wrap (FW) (Fig. 2b), Side Bond (SB) (Fig.
162 2c), and U-wrap with FRP Anchor (FA) (Fig. 3). As an example, P4-025-SB stands for the
163 specimen with #4 transverse rebar, 0.6 mm (0.025 in.) thick FRP sheets and side bond (SB)
164 wrapping scheme. REF-P3 and REF-P4, stand for RC reference specimens with No. 3 and 4
165 transverse rebar, respectively.

166 Standard material tests were conducted to obtain the material properties. Type III cement was
167 used for concrete casting. Standard 152 mm × 305 mm (6 x 12 inch) cylinders were tested to
168 obtain the compressive strength of concrete $f_c^{'}$ as per ASTM C39 [31]. The FRP sheets were
169 made of unidirectional carbon fibers with the material properties determined from coupon tests
170 per ASTM D3039 [32]. The wet lay-up system was used for installation of FRP sheets. The
171 specimen was ground, sandblasted, and power-washed to provide the proper concrete surface
172 conditions that would develop the necessary bond strength between the concrete and FRP sheets.
173 Putty and primer were first applied on the surface; the sheets were then impregnated with epoxy
174 resin and applied in-situ. Specimens were then cured for a minimum of 72 hours before testing. .
175 Along with preparing each specimen, a concrete beam was cast and FRP was applied to test the
176 pull-off strength of the FRP-concrete interface. To have a quality control of the bond strength of
177 the FRP-concrete interface, the standard pull-off tests were carried out by using the Dyna Z16
178 pull-off tester. The test follows the requirements of ASTM D7522 [33]. Before the pull-off test,
179 several 2 in. diameter cores were cut by a core drill, then the 2 in. diameter aluminum disks were
180 attached onto the FRP sheets by high strength epoxy, with manufacture tested strength of 1500
181 psi. When testing, the disk was attached to the pull-off tester and the pull-off load was applied by
182 the manual crank. The ultimate load was captured by the load indicator and used to calculate the
183 pull-off strength. The pull-off strength, σ_p shall be at least 1.4 MPa [1]. Details of the respective

material properties of steel and FRP are presented in Table 1, where E_{ls} and $E_{ts}$are the steel modulus of Elasticity in *l* and *t* directions, respectively; and E_f are the modulus of elasticity of steel and FRP, respectively; ρ_t and ρ_l are the steel reinforcement ratios in *l* and *t* directions, respectively; and f_y is the yielding strength of steel.

Loading Method and Instrumentation

Proportionally applied tensile load (horizontal σ_1) and compressive forces (vertical σ_2) were used to simulate a pure shear loading condition in the experimental test. As shown in Fig. 4, the reference *l*-*t* coordinate system represents the directions of longitudinal and transversal reinforcements. The reference 1-2 coordinate system represents the directions of the principal compressive stress (2-axis) and tensile stress (1-axis). Testing initially started using load control with increments of 1 kN/min. up to first cracking and then switched to displacement control with the increment of strain in the horizontal direction set to 0.0001 (mm/mm)/min until the specimen failed.

The average (smeared) strains in the horizontal, vertical, and diagonal directions were measured by a total of 14 Linear Variable Differential Transformers (LVDTs) attached on both sides of the panel specimen. With the stable reading from LVDTs, the stress-strain curves of concrete panels in the post peak branches were reliably monitored. On the North side, the panel specimen was instrumented symmetrically by 10 LVDTs. Four of the LVDTs were aligned horizontally, and another set of 4 LVDTs were aligned vertically, and each one of the remaining two was aligned along a diagonal direction as shown in Fig. 5a. On the south side of the specimen, four LVDTs were used: two in horizontal direction and two in vertical direction (Fig. 5b). The gage length for horizontal and vertical LVDTs was 800 mm, and gage length for diagonal LVDTs was 1,130 mm.

The local strains on steel rebar and FRP sheets for each panel specimen were measured by a total of 10 strain gauges. The position of strain gauges on steel rebar and FRP sheets are shown in Fig. 6 and Fig. 7, respectively. It should be noted that the strain gauges on steel and FRP were located at the same location.

A digital image correlation (DIC) system was used to obtain the displacement and deformation field on the south side of the specimen. Through this DIC-based non-contact measurement system, the crack spacing and crack width of the specimens were captured in real time. Load was measured by the load cells installed on each hydraulic actuator.

GENERAL BEHAVIOR OF TEST PANELS

The specimens were subjected to pure shear loads in the *l-t* coordinates, as shown previously in Fig. 4. The peak stresses and strains for all the test panels are listed in Table 2. The subscript "m" indicates the load stresses at the peak shear stress and the subscript "0" indicates the strains that are measured at the peak shear stress.

The shear stress, τ_{lt}, can be calculated in terms of the principle stress from Eq. (1) and the shear strain, γ_{lt},is determined form Eq. (2) as follows:

$$\tau_{lt} = \frac{1}{2}(\sigma_1 - \sigma_2) \quad (1)$$

$$\gamma_{lt} = \varepsilon_1 - \varepsilon_2 \quad (2)$$

where σ_1 and σ_2 are the average horizontal tensile and vertical compressive stresses, respectively; ε_1 and ε_2 are the average strains measured from LVDTs in horizontal and vertical directions, respectively.

Effect of FRP Stiffness on the Shear Behavior

To study the shear behavior of FRP-strengthened RC members and to investigate the effect of FRP stiffness, panels with same steel reinforcements in *l* and *t* directions, but different FRP reinforcement ratios are tested. The application of FRP in the *t*-direction results in an increase of effective reinforcement ratio in that direction. The effective reinforcement ratio is defined as the contribution of transverse steel and FRP reinforcement ratio in the shear gain in *t* direction. Therefore, a different behavior is expected to be observed. To compare the behavior of panels, the shear stress-strain curves of panels series P4-FW, with the same steel reinforcement ratio in *l* and *t* directions ($\rho_l = \rho_t = 0.76\%$) and different FRP reinforcement ratios (FRP Stiffness) fully wrapped, are shown in Fig. 8. It can be observed that with the increase of FRP stiffness, the shear strength of panels increases. The maximum shear strength of test panels P4-025-FW, P4-040-FW, and P4-080-FW were 4.2 MPa, 5.6 MPa, and 6.3 MPa, respectively. With the increase of FRP stiffness, the stiffness of strengthening system increases and the contribution of FRP reinforcement to shear capacity will increase; therefore, the shear strength of panels increases. The presence of FRP sheets along the transverse direction delays the yielding of steel rebar in the *t*-direction. Therefore, the rebar in the longitudinal direction will yield sooner compared to the rebar in the transverse direction. In other words, the rebar in *l* and *t* directions will not yield at the same time as in panel REF-P4.

In order to compare the behavior of panels, the relationships between the shear stress and average strain in longitudinal and transverse directions of panels series P4-FW are shown in Fig. 8. Panel REF-P4 is reinforced with equal amount of steel in *l* and *t* directions. Due to symmetry of the loading and the reinforcements, the average strain in the *l*-direction, ε_l, equals the average strain in the *t*-direction, ε_t. Therefore, the steel in both directions approximately yielded at the same time. Also, the inclination of cracks in this case coincides with the direction

of principal compressive stress. Therefore, the interlocking action of aggregates between concrete struts vanishes. As shown in Fig. 9, the measured strains in the two directions for panel REF-P4 are very close to each other from the beginning of testing up to failure of the panel. Panels in series P4-FW were reinforced with equal amount of steel in *l* and *t* directions ($\rho_l = \rho_t = 0.76\%$). However, they were strengthened with different FRP reinforcement ratios along the *t*-direction. Therefore, the presence of FRP sheets resulted in the increase of the effective reinforcement ratio in transverse (*t*) direction and the steel in *l*-direction yielded sooner than the steel in *t*-direction (Fig. 9). After steel yielded in both *l* and *t* directions, the average strain in longitudinal direction ε_l increased rapidly compared to the average strain in transverse direction ε_t. The FRP sheets aligned in the *t*-direction prevented the rapid increase of strain along the transverse direction. It is observed from Fig. 9 that with the increase of FRP stiffness, the difference in steel strains in *l* and *t* directions increases. For instance, in panel P4-025-FW, ε_l at failure is 20% more than ε_t. With the increase of FRP reinforcement ratio this difference increases. In panels P4-040-FW ($\rho_f = 0.87\%$) and P4-080-FW ($\rho_f = 1.74\%$), ε_l at failure is greater than ε_t by 53% and 60%, respectively. With the increase of FRP reinforcement ratio (FRP stiffness) in the transverse direction, the effective reinforcement ratio in the *t*-direction increases. This will result in increase of deformation in the *l*-direction which is less reinforced.

Effect of Wrapping Scheme on the Shear Behavior

Wrapping scheme affects the confinement effect of the FRP sheets and the potential for debonding. The effect of wrapping scheme on the shear stress-strain curves of the panels are shown in Fig. 10 and Fig. 11. Test results of panels with the same steel and FRP reinforcement ratios ($\rho_s = 0.76\%$, $\rho_f = 0.87\%$), but different wrapping schemes are shown in Fig. 10. The behavior of panel P4-040-SB was similar to panel P4-040-FA up to failure. However, the shear

capacity of panel P4-040-FA was 22% greater than panel P4-040-SB. Panel P4-040-SB failed due to premature debonding of FRP sheets. Panel P4-040-FW showed a different behavior compared to the other two panels. The stiffness of the panel P4-040-FW after cracking was much higher compared to P4-040-FA and P4-040-SB panels, which showed the same post cracking behavior. This was due to a better bond between the FRP sheets and concrete substrate after cracking of concrete in panel P4-040-FW, which resulted in the increase of the overall stiffness. The shear capacity of panel P4-040-FW was 6% and 30% higher than panels P4-040-FA and P4-040-SB, respectively. In Fig. 11, test results of panels with the same steel and FRP reinforcement ratios ($\rho_s = 0.76\%$, $\rho_f = 0.43\%$), but different wrapping schemes are compared. Although it was expected that the two panels show a similar behavior up to failure, the shear capacity of panel P4-025-FA was 15% higher than panel P4-025-FW. This difference was due to a lower concrete compressive strength, f_c', of panel P4-025-FW (45 MPa) compared to panel P4-025-FA (52 MPa). The contributions of steel and FRP on the overall shear capacity of the two members were similar. However, the lower concrete compressive strength resulted in a lower contribution of concrete on the overall shear capacity of panel P4-025-FW therefore, a lower overall shear capacity was observed compared to panel P4-025-FA.

For design purposes, the strengthening scheme is selected based on factors such as the accessibility of the member and the required amount of increase in shear capacity. The recommended wrapping scheme is fully wrap for shear strengthening of the member whenever it is possible. However, in most situations, a U-wrap with FRP anchor is the only economical and practical economical and practical wrapping scheme.

Effect of Transverse Steel Reinforcement on the Shear Behavior

297 The panels were reinforced with two levels of transverse steel reinforcement ratios,
298 ρ_t = 0.43% and 0.76%. A low transverse reinforcement ratio (using No. 3 rebar) was chosen to
299 simulate a beam which is lightly reinforced, and a high transverse reinforcement was chosen to
300 simulate a beam which is heavily reinforced. The shear stress-strain curves of panels with the
301 same FRP reinforcement ratio and wrappings scheme, but different transverse reinforcement
302 ratios are compared in Figs. 12 and 13. The shear stress-strain curves of panels P3-040-FW and
303 P4-040-FW are compared in Fig. 12. The panels are reinforced with the same FRP reinforcement
304 ratio (ρ_f = 0.87%) and the wrapping scheme is fully wrap. It can be observed that panel P4-040-
305 FW had 25% higher shear strength compared to panel P3-040-FW, due to a higher transverse
306 reinforcement ratio.

307 In Fig. 13, the shear stress-strain curves of panels P3-025-FW and P4-025-FW are compared.
308 The panels are reinforced with the same FRP reinforcement ratio (ρ_f = 0.54%) and the wrapping
309 scheme is fully wrap. The two panels showed similar behavior in terms of maximum shear stress.
310 It was expected that panel P4-025-FW show higher shear strength compared to panel P3-025-
311 FW. Although, panel P4-025-FW had a lower concrete compressive strength (f_c' = 45 MPa)
312 compared to panel P3-025-FW (f_c' = 51 MPa), panel P3-025-FW reached its peak strength at a
313 lower shear stress and strain compared to panel P4-025-FW.

314 In Fig. 14, the strain of FRP sheets and transverse steel, measured using strain gauges, for panels
315 P4-040-FW and P3-040-FW are compared at same load levels. It is observed that both the
316 external FRP reinforcement and the transverse steel reinforcement did not contribute to the load-
317 carrying capacity in the initial stage of loading. This contribution initiated and became effective
318 after the first cracking occurred. In panel P4-040-FW it can be observed that before reaching the
319 tensile strength of concrete, the strains in FRP and steel were very small and less than the

maximum tensile strain of concrete. Once cracking occurred, strains on both steel and FRP increased suddenly. Before yielding of the steel, FRP strain was higher than the steel strain at the same load level. After steel yielded, the steel strain rapidly increased compared to FRP strain. The same behavior was observed for panel P3-040-FW. In panel P3-040-FW immediately after the steel yielded, since the transverse steel reinforcement ratio was low, the steel strain increased rapidly and became higher than FRP strain at the same shear stress level. In panel P4-040-FW, immediately after steel yielded, the transverse steel strain did not get bigger than the strain of FRP. This was due to a larger steel reinforcement ratio compared to panel P3-040-FW, and due to the different yield behavior of rebar Nos. 3 and 4 compared to each other. The strains in the FRP and the transverse steel are different, even at the same locations, because the strain on the fiber sheets increases drastically near the crack, due to the bond between the FRP and the concrete substrate. Also, the crack widths are smaller at the rebar location and increase at the surface. Addition of the FRP sheets delayed the contribution of transverse steel to the load carrying capacity of the specimen. The results clearly show that the effect of externally bonded FRP sheets preserves the integrity of internal transverse steel reinforcements. The effectiveness of the contribution of FRP sheets to the shear gain highly depends on the amount of internal shear steel reinforcement. However, the design guidelines have not yet considered the effect of transverse steel reinforcement and the contribution of FRP on the overall shear response (V_f) in their formulations.

Failure Modes Associated with FRP-Strengthened RC Panels

In RC members subjected to compression-tension biaxial stresses, various types of shear failure occur; such as diagonal cracking, splitting, shear-compression failure, and web crushing[15]. These all involve cracking and crushing of concrete in a biaxial stress state. In FRP-strengthened

RC members, additional failure modes were observed. The two main failure modes related to the FRP strengthening which were observed in test panels are FRP rupture and FRP debonding. In the case of FRP rupture, the fibers reached their ultimate strain value and fracture at the point of maximum stress. In the FRP debonding failure mode, the strain of FRP at ultimate stage were considerably lower than the rupture strain. The failure mode of FRP rupture is similar to shear tension failure in conventional RC beams where vertical flexural cracks originates from the tension face. Widening of the diagonal crack eventually leads to failure involving tearing of the FRP along a line corresponding to the diagonal shear crack in the concrete. Available experimental data in literature shows that all of the test specimens with FRP sheets bonded on sides only, and many bonded with U-wrap, failed by debonding of the FRP from the concrete substrate.

The main failure modes associated to panel specimens are shown in Table 3. Fig. 15 shows the main failure modes observed in panel specimens. In panels P3-FW and P4-FW series, which were strengthened with fully wrap scheme, the main observed failure modes were FRP rupture followed by crushing of concrete (Fig. 15a), except for panel P4-080-FW which failed by concrete crushing prior to FRP failure (Fig. 15b). Concrete crushing occurred due to high principal compressive stresses in the region between induced cracks. This failure mode is normally associated with high amounts of transverse reinforcement but may also be critical in beam members with thin webs. Panel P4-080-FW, which was strengthened with a higher FRP reinforcement ratio compared to other panels (ρ_f = 1.74%), had a different failure mode. The governing failure mode in this panel was concrete crushing. The increase in amount of FRP reinforcement (increase in thickness of FRP sheets) resulted in decrease of active bond length, that is the length which the majority of bond is maintained. Therefore, the effective strain in the

FRP sheets decreases and ultimately, FRP sheets did not reach their expected capacity up to their tensile strength before rupture and the panel failed due to concrete crushing.

In panels P4-FA series, which were strengthened using U-wrap with FRP anchor wrapping scheme, a mixed failure mode was observed. In panel P4-025-FA, anchorage failure was observed on the south side of the panel while on the north side FRP rupture of FRP sheets was seen (Fig. 15c). In panel, P4-040-FA, FRP anchors did not show any sign of failure and the failure mode of the panel was governed by rupture of FRP sheets. This could be associated with different bond between FRP and concrete substrate on both sides of the panel. On the south side of the panel, the FRP anchors engaged in the shear resistance once the FRP sheets debonded from the concrete surface and failed at their ultimate load carrying capacity.

Panel P4-040-SB, was strengthened with the side bond wrapping scheme. Once the concrete cracked, local debonding of FRP sheets initiated from the concrete substrate and the panel ultimately failed by debonding of all FRP sheets at a lower load level compared to other strengthened panels (Fig. 15d). In this panel, the FRP was not able to utilize its full tensile capacity and therefore, debonding of FRP sheets at lower strain levels occurred, which lowered the efficiency of the strengthening system. In this mode of failure, once the FRP starts to peel off, the beam will fail very quickly in a brittle process. The bond strength between FRP and concrete thus plays the key role in this mode.

It should be noted that the strain distribution in the FRP along a shear crack is non-uniform because the width of the critical shear crack changes from the lower end to the upper crack tip [34]. This leads to a non-uniform strain distribution in the FRP because the strain anywhere in the FRP intersected by the crack is closely related to the width of the crack at that location. Since the FRP sheets are linear elastic material up to their rupture, the stress in the FRP is also non-

389 uniform along the shear crack. Combined with the brittle behavior of FRP, this means that at
390 any instant in the failure process, only the most highly stressed part of the FRP is at its full
391 tensile capacity.

392 In practice, for design of FRP strengthened RC members, the primary failure modes are
393 selected for each element. Each failure mode is classified in terms of the type of failure it
394 represents and the seriousness of damage it causes [35]. A primary failure mode should be
395 considered followed by other failure modes and their degree of undesirability. For instance, in an
396 RC beam strengthened with FRP, the most desirable failure mode is flexural concrete crushing
397 and the least desirable is debonding. For shear strengthening, the failure modes and bond of
398 FRP to concrete substrate remain the focus of many research work. There are several verities in
399 failure modes in FRP strengthened systems which can govern the strength [1]. While most of the
400 failure modes have been identified by researchers, more accurate methods are still required.
401 Throughout the design procedures, significant limitations on the strain and stress level achieved
402 in the FRP material are imposed to conservatively account for debonding failure modes. More
403 thorough design guidelines should be incorporated in codes for predicting debonding and other
404 failure modes.

405
406 **CRACK CHARACTERISTICS**

407 The evolution of strains and deformations on FRP and concrete have been measured with a DIC
408 system and its tracking method. This method has been widely used for measurements in RC and
409 masonry members [36-38]. In order to study the crack characteristics on panel specimens, the
410 DIC system was used on the south side of the specimen. The DIC system will generate contour

411 plots of the axial and lateral surface deformations of the panels, which will help determine the
412 exact pattern around and in between the FRP sheets [19].

413 The crack characteristics including crack width, spacing, and amount were measured by the DIC
414 system and are presented in the following sections. In Fig. 16, the strain field in the direction of
415 applied horizontal load ε_x of a specimen at a specific load level is shown using color gradient.
416 The cracks are identified at locations with sudden increase in strain. The crack widths are
417 measured by assigning two points near the cracks and continuously measuring their distances. It
418 should be mentioned that due to accessibility issue, the DIC system was not used for specimen
419 P4-025-FW, P4-040-FA, and P4-040-SB. The integrity of a structure is affected by the crack
420 characteristics and therefore careful considerations should be made [39].

421 **Crack Spacing**

422 The stabilized cracking phase is reached when the crack spacing between two existing
423 cracks are too small for a new crack to develop in between. The crack spacing was determined at
424 the last phase of the testing, since it is closest to the stabilized cracking stage. In Table 4,
425 experimental measurements of the average crack spacing, S_{rm}, maximum crack spacing, $S_{r,max}$,
426 and minimum crack spacing, $S_{r,min}$, in panel specimens subjected to shear are presented. The
427 experimental average crack spacing is defined by the measurement of the spacing between the
428 adjacent cracks on the panel at different heights and averaging for the entire specimen at the
429 stabilized cracking stage. The maximum and minimum crack spacing is defined based on the
430 maximum and minimum measured crack spacing at the stabilized cracking stage throughout the
431 specimen, respectively. In Fig. 17, ratios of maximum and minimum to average crack spacing
432 versus average crack spacing in shear tests of panel specimens are presented. The mean value of
433 the ratio $S_{r,max}/S_{rm}$ and $S_{r,min}/S_{rm}$ are shown with horizontal dashed lines. In EC2-04 [40] a value

of 1.7 is assumed for the ratio of the maximum to average crack spacing for RC structures; which is observed to be higher compared to the experimental value of $S_{r,max}/S_{rm}$ that equals 1.47 for FRP-strengthened RC panels.

Crack Width

Using the DIC system the crack widths were measured continuously during the test. It was observed that in FRP-strengthened RC members; average crack widths were generally smaller than for un-strengthened members at the same shear strain level (Fig. 18), due to the additional bond action developing at the FRP-concrete interface. Although, the number of cracks did not increase significantly in strengthened members as shown in Table 4., the crack widths decreased compared to RC panels. The thicker FRP (1.0 mm) provided better crack control compared to the thinner FRP (0.6 mm). Similar results were observed for P4-FW and P4-FA series. As shown in Fig. 19, in panels strengthened with FRP, average crack widths were generally smaller than un-strengthened RC panels at the same shear strain level. For panels P4-FW series, with the increase of FRP reinforcement ratio, the crack widths did not change significantly at lower shear strains. In general. specimens strengthened with FRP exhibited a greater tension stiffening effect compared to RC specimens. The contribution of the concrete in shear affects the overall stiffness of the FRP strengthened RC members after cracking. Therefore, the crack spacing and crack width are affected at service load level. Wrapping scheme and FRP reinforcement ratio affect the bond behavior of steel-concrete and, FRP-concrete interface in FRP strengthened RC members. This will result in a different crack pattern in such members compared to RC members.

MATHEMATICAL MODELING OF SMEARED STRESS-STRAIN CURVES OF FRP STRENGTHENED RC IN COMPRESSION

The softening coefficient is the most important parameter affecting the smeared stress-strain relationships of concrete in compression. Several researchers have investigated the softening coefficient in RC members and determined that the most effective parameters are: concrete compressive strength, f_c', the uniaxial tensile strain, $\bar{\varepsilon}_1$, and the deviation angle, β [13,14]. In case of FRP strengthened RC members, the FRP sheets also have significant effect on the softening of concrete [16]. The smeared constitutive relationship of concrete compressive stress, σ_2^c, versus the uniaxial compressive strain, $\bar{\varepsilon}_2$, in the Softened Membrane Model, shown in Fig. 20, is given as:

$$\sigma_2^c = \zeta f_c' \left[2\left(\frac{\bar{\varepsilon}_2}{\zeta\varepsilon_0}\right) - \left(\frac{\bar{\varepsilon}_2}{\zeta\varepsilon_0}\right)^2 \right] \quad \text{when } \frac{\bar{\varepsilon}_2}{\zeta\varepsilon_0} \le 1 \text{ and} \tag{2}$$

$$\sigma_2^c = \zeta f_c' \left[1 - \left(\frac{\left(\bar{\varepsilon}_2 / \zeta\varepsilon_0\right) - 1}{\left(4/\zeta\right) - 1} \right)^2 \right] \quad \text{when } \frac{\bar{\varepsilon}_2}{\zeta\varepsilon_0} > 1 \tag{3}$$

The softening coefficient in Eq. 2 and 3 is expressed as the product of the function of concrete compressive strength, f_c', uniaxial tensile strain, $\bar{\varepsilon}_1$, and deviation angle, β, as

$$\zeta = f(f_c')f(\bar{\varepsilon}_1)f(\beta), \text{ where} \tag{4}$$

$$f(f_c') = \frac{5.8}{\sqrt{f_c'}} \le 0.9 \tag{5}$$

$$f(\bar{\varepsilon}_1) = \frac{1}{\sqrt{1+400\bar{\varepsilon}_1}}, \tag{6}$$

$$f(\beta) = 1 - \frac{|\beta|}{24^o} \tag{7}$$

Previous researches showed that in FRP strengthened RC members, FRP reinforcement has

475 significant effect on the softening coefficient [9 ,16]. Therefore, in FRP strengthened members
476 the softening coefficient is expressed as

477 $$\zeta_{FRP} = f(f_c')f(\bar{\varepsilon}_1)f(\beta)f(FRP) \quad (8)$$

478 where, the first three terms on the right-hand side of Eq. (8) are the same as the
479 softening coefficient for RC, Eq`ns. (5) to (7), proposed by other researchers at
480 University of Houston [14, 18,41]. The fourth term is proposed by Yang [9] as

481 $$f(FRP) = 1 + 0.0076\sqrt{\rho_f E_f} \quad (9)$$

482 In the proposed equation, $\rho_f E_f$ were adopted to account for the area of the
483 concrete. It should be noticed that the proposed equation converges to the result of
484 RC when $\rho_f E_f$ equals to zero, in which case f (FRP) equals to 1 and the expression
485 will be the same as for RC.

486 To express the smeared stress-strain curves of the concrete in compression in
487 FRP strengthened RC members, the same parabolic equation, Eq. (2) and (3), is
488 used. The softening coefficient is derived from Eq. (8). The experimental results of
489 FRP strengthened RC panels subjected to shear will be used to validate the function
490 of deviation angle, β, in the softening equation of RC members for FRP
491 strengthened RC members.

492 The angle β is the deviation angle between *r*-*d* coordinate and 1-2 coordinate,
493 equal to α_r-α_1 (Fig. 21). β is a function of the strain state, and can be expressed in
494 terms of the three strains, ε_1, ε_2, and γ_{12} using the compatibility equations as

495 $$\beta = \frac{1}{2}\tan^{-1}\left[\frac{\gamma_{12}}{\varepsilon_1 - \varepsilon_2}\right] \quad (10)$$

The deviation angle, β, is equal to zero if the element is reinforced with the same amounts of steel bars in *l* and *t* directions and subjected to pure shear loading, e.g., REF-P4. The values of β and $f(\beta)$ from FRP strengthened RC panel tests are listed in Table 5. The concrete compressive strength, f_c', and the uniaxial tensile strain, $\bar{\varepsilon}_1$, of the concrete in the 1-direcrion at the peak point of the shear stress-strain curve for each panel are listed in Table 5. The values of $f(f_c')$, $f(\bar{\varepsilon}_1)$ and $f(FRP)$ are calculated using Eqns. (5, 6, and 9), respectively. Dividing the experimental value of the softening coefficient, ζ_{exp}, by $f(f_c')$, $f(\bar{\varepsilon}_1)$, and $f(FRP)$ the experimental $f(\beta)$ for each panel is obtained and listed in Table 5. The value of β for each panel is calculated using Eq. (10).

According to the data in Table 5, the $f(\beta)_{exp}$ versus β relationships for the FRP strengthened RC panels is plotted in Fig. 20 along with the data for the reinforced concrete panel tests [18, 41]. Also, the straight line defined by Eq. (7) is plotted in Fig. 20.

The $f(\beta)_{exp}$ versus β relationships for FRP strengthened RC panels show a different trend than that for RC panels. Therefore, Eq. (7) should be modified before it can be applied to FRP strengthened RC members. Similar to RC members, the relationship between β and $f(\beta)$ is approximately linear. A regression analysis of the FRP strengthened RC data is performed to develop the new function of the deviation angle, β, in the softening coefficient of FRP strengthened RC members as

$$f_{FRP}(\beta)=\left(1-\frac{|\beta|}{16^{o}}\right) \quad (11)$$

The effect of deviation angle, β, on the softening coefficient in FRP strengthened RC members is more complicated than that in RC members. The presence of FRP along the transversal direction increases the stiffness in that direction and therefore, increases the difference in the stiffness in the *l* and *t* directions. Thus, the deviation angle increases followed by a decrease in the softening coefficient. The new function of the deviation angle, $f_{FRP}(\beta)$, has been used for the softening equation of the new softened membrane model for FRP strengthened RC members presented elsewhere [42].

CONCLUSIONS

In order to evaluate the shear behavior of FRP-strengthened RC members and investigate the main factors which influence its behavior, panel testing was carried out. Other testing techniques such as testing beam with various a/d ratios cannot predict the true pure shear behavior due to the presence of flexural and other non-shear related effects that cannot be filtered out. For this purpose, full-scale tests on 8 FRP-strengthened RC panels and 2 RC panels were conducted. It should be noted that in this research the initial stresses existing in members prior to strengthening have been considered. The effects of different parameters on the true shear behavior of FRP-strengthened RC members were investigated. The following conclusions can be made:

1) It was found that the application of FRP sheets enhanced the overall shear behavior of RC panels. However, ductility of the specimens was reduced due to the failure modes associated with the strengthening system such as FRP rupture and FRP debonding.

2) The presence of FRP sheets resulted in the increase of the effective reinforcement ratio in transverse direction, and the steel in the *l*-direction yielded sooner than the steel in the *t*-direction. After the steel yielded in both *l* and *t* directions, the strain in the longitudinal direction, ε_l, increased rapidly compared to the strain in the transverse direction, ε_t. The FRP sheets aligned in the *t*-direction prevented the rapid increase of strain along the transverse direction. Also, with the increase of FRP reinforcement ratio, the difference in steel strains in *l* and *t* directions increased.

3) In this research, many failure modes of FRP strengthened RC members have been identified. While some of these failure modes are similar to those of RC members, others are unique to FRP strengthened members. The transfer of stresses from concrete to FRP sheets is a critical parameter in FRP strengthening since it is likely to cause undesirable premature and brittle failures. The two main failure modes observed in the tests were rupture of FRP sheets at the ultimate strain following the yielding of internal steel reinforcement and debonding of FRP sheets in a brittle manner with a thin layer of concrete residue attached to the delaminated FRP sheet. It was observed that wrapping schemes played a critical role in determining the failure mode of the strengthened member. While all specimen with side bond wrapping scheme failed by premature FRP debonding, most specimens with U-wrap plus FRP anchor and fully wrap failed by concrete crushing followed by rupture of FRP.

4) It was observed that the magnitude of increased shear capacity associated with the application of FRP sheets depend not only upon the amount of FRP reinforcement that is being used, but also on the amount of internal shear reinforcement. The increase in transverse steel reinforcement resulted in a significant decrease in the shear gain due to FRP strengthening. There exists a high

interaction between the components of the strengthening system, specifically steel and FRP reinforcement, when subjected to shear. The strains in the FRP sheets and the internal transverse steel reinforcement were observed to be different at the same locations in the test region. This was due to the strain on the fiber sheets increasing drastically near the cracks, due to the bond between the FRP and the concrete substrate. With increase in the internal shear reinforcement ratio, the crack pattern becomes relevantly more distributed along the member and therefore, the available effective bond length decreases. This ultimately leads to decrease in the bond force and decrease in the effectiveness of the FRP strengthening scheme. It should be noted that the external FRP reinforcement does not prevent the internal transverse steel reinforcement from yielding rather delays it.

5) Test results showed that applying FRP reinforcement significantly changed the crack width and spacing of the RC member. The contribution of the concrete in shear affects the overall stiffness of the FRP strengthened RC members after cracking. Therefore, the crack spacing, and crack width are affected at service load level. Different wrapping schemes and external FRP reinforcement ratio affects the bond behavior of steel-concrete and also FRP-concrete interface in FRP strengthened members. This will result in different crack patter in in such members compared to RC members. Average crack widths were generally smaller than for un-strengthened RC members at the same smeared strain level due to the additional bond action developing at the FRP-concrete interface which further reduced the crack spacing.

6) The softening coefficient is the most important parameter affecting the smeared stress-strain relationships of concrete in compression. Previous research studies showed that in addition to effective parameters in the softening coefficient of RC members, FRP sheets also have significant effect on the softening of concrete in FRP strengthened RC members. In this paper, a

new softening coefficient for FRP strengthened reinforced concrete in compression is proposed based on panel tests. The new softening coefficient includes the modified deviation angle factor in terms of the deviation angle β. The presence of FRP along the transversal direction increases the stiffness in that direction and therefore, increases the difference in the stiffness in the *l* and *t* directions. Thus, the deviation angle increases followed by a decrease in the softening coefficient. The new function of the deviation angle was implemented in the softening equation of the new softened membrane model for FRP strengthened RC members presented elsewhere.

ACKNOWLEDGEMENTS

This research was supported by the National Science Foundation, award number 1100930. Steel reinforcement and FRP materials were donation from GERDAU AMERISTEEL Co. and FYFE. Co, respectively. Their support is greatly acknowledged.

REFERENCES

[1] ACI Committee 440. Guide for the design and construction of externally bonded FRP systems for strengthening concrete structures. ACI 440.2R-08. Farmington Hills (MI): American Concrete Institute; 2008.

[2] A. Khalifa, A. Nanni. Improving shear capacity of existing RC T-section beams using CFRP composites. Cem. Conc. Compos., 22(2000) 165-174.

[3] H. Baghi, JA. Barros, F. Menkulasi. Shear strengthening of reinforced concrete beams with Hybrid Composite Plates (HCP) technique: experimental research and analytical model. Eng. Struct. 125(2016) 504–20.

[4] B. B. Adhikary, H. Mutsuyoshi, M. Ashraf. Shear strengthening of reinforced concrete beams using fiber-reinforced polymer sheets with bonded anchorage. *ACI Struc. J.* 101(2004)

660-668.

[5] AASHTO. AASHTO LRFD Bridge design specifications. Washington, DC. 2008.

[6] A. Belarbi,, S.W. Bae, A. Ayoub, D. Kuchma, A. Mirmiran, A. Okeil. Design of FRP systems for strengthening concrete girders in shear. *NCHRP Rep. No. 678* Washinton D.C. 2011.

[7] M.A. Colalillo. Behavior of shear-critical reinforced concrete beams retrofitted with externally applied fibre-reinforced polymers (Doctoral dissertation). Department of Civil Engineering, University of Toronto, Toronto, Canada. 2012.

[8] A. Mofidi, O. Chaallal. Effect of steel stirrups on shear resistance gain due to externally bonded fiber-reinforced polymer strips and sheets. ACI Struc. J. 111(2014) 353–361.

[9] G.Yang, M. Zomorodian, A. Belarbi, A. Ayoub A. Uniaxial Tensile Stress-Strain Relationships of RC Elements Strengthened with FRP Sheets. J. Compos. Constr., 2015. 10.1061/(ASCE)CC.1943-5614.0000639, 04015075.

[10] H. Baghi, J.A. Barros. Shear strengthening of reinforced concrete T-beams with hybrid composite plate. J. Compos. Constr., 20.6 (2016): 04016036.

[11] G. Monti, M.A. Liotta. Tests and design equations for FRP-strengthening in shear. *Construction and Building Materials*, 21(2007) 799-809.

[12] V. Colotti, R.N. Swamy. Unified analytical approach for determining shear capacity of RC beams strengthened with FRP. Eng. Struct. 33(2011) 827-842.

[13] T.T.C. Hsu, R.R.H. Zhu. Softened Membrane Model for reinforced concrete elements in shear Struc. J. ACI. 99(2002) 460–469.

[14] A. Belarbi, T.T.C. Hsu. Constitutive laws of concrete in tension and reinforcing bars stiffened by concrete. ACI Struc. J. 91(1994) 465-474.

631 [15] T.T.C. Hsu, Y.L. Mo. Unified theory of concrete structures. West Sussex, UK: John Wiley
632 and Sons Ltd. 2010.
633 [16] G. Yang, M. Zomorodian, A. Belarbi. Material Laws of FRP-Strengthened RC Element in
634 Biaxial Tension–Compression. *J. Compos. Constr*. 2017. 10.1061/(ASCE)CC.1943-5614.
635 20170000804.
636 [17] T.T.C. Hsu, L.X. Zhang, T. Gomez. A Servo-Control System for Universal Panel Tester. J.
637 Test. Eval., 23 (1995) 424–430.
638 [18] Pang, X. B., Hsu, T. T. C. (1996). Fixed-Angle Softened-Truss Model for reinforced
639 concrete. ACI Struct. J., l, 93(2), 197-207 [19] M. Zomorodian, G.Yang, A. Belarbi, A.S.
640 Ayoub. Cracking behavior and crack width predictions of FRP-strengthened RC members
641 under tension. *Eng. Struct.,* 125(2016) 313-324.
642 [20] A. Bousselham, O. Chaallal. Shear strengthening reinforced concrete beams with fiber-
643 reinforced polymer: assessment of influencing parameters and required research. *ACI Struc.*
644 *J.* 101(2004) 219–227.
645 [21] A. Bousselham, O. Chaallal. Effect of transverse steel and shear span on the performance of
646 RC beams strengthened in shear with CFRP. *Compos. Part B: Eng.*, 37(2006) 37–46.
647 [22] CAN/CSA S806-12. *Design and construction of building structures components with Fiber-*
648 *Reinforced Polymers.* Rexdale, Ontario, Canada. 2012.
649 [23] FIB (International Federation for Structural Concrete). FRP as externally bonded
650 reinforcement of R.C. structures: basis of design and safety concept. *Fib Bulletin 14*,
651 Lausanne, Switzerland. 2001.
652 [24] Triantafillou, T. C. (1998). "Shear strengthening of reinforced concrete beams using epoxy-
653 bonded FRP composites." *ACI Struc. J., 95*(2), 107–115.

654 [25] N. Eshwar, A. Nanni, T. Ibell. CFRP strengthening of concrete bridges with curved soffits.
655 *Proc., Int. Conf. on Structural Faults and Repairs*, Montreal, Quebec. 2003.
656 [26] G. Özdemir. *Mechanical properties of CFRP anchorage* (Master's Thesis). Department of
657 Civil Engineering, Middle East Technical University, Turkey. 2005.
658 [27] S.L. Orton. *Development of a CFRP system to provide continuity in existing reinforced*
659 *concrete buildings vulnerable to progressive collapse* (Doctoral dissertation). Department
660 of Civil, Architectural, & Environmental Engineering, University of Austin-Texas, Austin,
661 TX. 2007.
662 [28] Y. Kim, K. Quinn, J. Garcia,W. Sun, W. Ghannoum, J. Jirsa. *Shear strengthening of*
663 *reinforced and prestressed concrete beams using carbon fiber reinforced polymer (CFRP)*
664 *sheets and anchors (Technical Rep. 0-6306-1).* Austin, TX. 2012.
665 [29] K. Kobayashi,S. Fujii,Y. Yabe, H. Tsukagoshi, T. Sugiyama. Advanced wrapping system
666 with CF anchor-stress transfer mechanism of CF anchor. *Proc., of the 5th Int. Symp. on*
667 *FRP Reinf. for Conc. Struc. (FRPRCS-5).* Cambridge. UK. 2001.
668 [30] E. Grande, M. Imbimbo, A. Rasulo. Effect of transverse steel on the response of RC beams
669 strengthened in shear by FRP: experimental study. *J. Compos. Constr.*, *13*(2009) 405-414.
670 [31] ASTM. Standard test method for compressive strength of cylindrical concrete specimens.
671 ASTM C39, West Conshohocken, PA. 2014.
672 [32] ASTM. Standard test method for tensile properties of polymer matrix composite materials.
673 ASTM D3039, West Conshohocken, PA. 2014.
674 [33] ASTM. Standard test method for pull-off strength for FRP bonded to concrete substrate.
675 ASTM D7522, West Conshohocken, PA. 2014.
676 [34] G. Chen, J. Teng, J. Chen. Shear strength model for FRP-strengthened RC beams with

adverse FRP-steel interaction. *J. Compos. Constr*. 17(2013) 50-66.

[35] K. Neocleous, K.Pilakoutas, P. Waldron. Structural reliability for fibre reinforced polymer reinforced concrete structures. *Proc. of the 4th Int. Symp. on Fibre Reinf. Polymers for Reinf. Conc. Struc.* (FRPRCS-4). Baltimore. Maryland. 65-74. 1999.

[36] M.M.R. Mousavi, M.D. Champiri, M.S. Joshaghani, S. Sajjadi. A kinematic measurement for ductile and brittle failure of materials using digital image correlation. *AIMS Mat. Sci.* 3(2016) 1759-1772.

[37] S. Beizaee,K.J. Willam, G. Xotta,R. Mousavi. Error analysis of displacement gradients via finite element approximation of digital image correlation system. *Proc., Of the 9th Int. Conf. on Frac. Mech. of Conc. and Conc. Struc*. (FraMCoS-9), Berkeley, CA. 2016.

[38] M.D. Champiri, S.H. Mousavizadegan, F. Moodi. A decision support system for diagnosis of distress cause and repair in marine concrete structures. *Comput. Concr.*, 9(2012) 99–118.

[39] M.D. Champiri, S.H. Mousavizadegan, F. Moodi. A fuzzy classification system for evaluating the health condition of marine concrete structures. *J. Adv. Concr. Technol.*, 10(2012) 95–109.

[40] Eurocode-2. *Eurocode 2: Design of Concrete Structures-Part 1: General Rules & Rules for Buildings*. Brussels, Belgium. 2004.

[41] Zhang, L. X., Hsu, T. T. C. (1998). Behavior and analysis of 100-MPa concrete membrane elements. J. Struct. Eng., 124(1), 24-34.

[42] M. Zomorodian, A. Belarbi, A. Ayoub (2017). Finite element model for predicting the shear behavior of FRP-strengthened RC members. Eng. Struct., 153(2017) 239-253.

Figure Captions

Fig. 1. Dimensions of test panels

Fig. 2. Layout and wrapping method of FRP sheets, a) FRP layout, b) Fully wrap, and c) Side bond wrapping scheme cross sections

Fig. 3. U-Wrap with FRP anchor details

Fig. 4. Proportional loading of panel in 1-2 directions

Fig. 5. LVDT arrangement for the panel specimens

Fig. 6. Strain gauge layout on steel rebar of panel specimens

Fig. 7. Strain gauge layout on FRP sheets of panel specimens

Fig. 8. Effect of FRP stiffness on shear stress-shear strain curves of panels P4-FW series

Fig. 9. Effect of FRP stiffness on $\tau_{lt} - \varepsilon_l$ and $\tau_{lt} - \varepsilon_t$ relationships of panels P4-FW series

Fig. 10. Shear stress-strain curves for specimens with different wrapping schemes (panels P4-040 series)

Fig. 11. Shear stress-strain comparison of wrapping scheme in panels P4-025 series

Fig. 12. Shear stress-strain comparison of transverse steel reinforcement in panels 040-FW series

Fig.13. Shear stress-strain comparison of transverse steel reinforcement in panels 025-FW series

Fig. 14. Comparison of transverse steel strain and FRP of panels P4-040-FW and P3-040-FW

Fig. 15. Different failure modes of panel specimens, a) FRP debonding, b) Concrete crushing, c) FRP anchor failure, d) FRP rupture

Fig. 16. Full strain field in the direction of applied load of specimen at a specific load level

Fig. 17. Ratios of maximum and minimum to average crack spacing vs. average crack spacing in shear tests

Fig. 18. Crack width comparison of panel series P3-FW and REF-P3

Fig. 19. Crack width comparison of panel series P4-FW and P4-FA

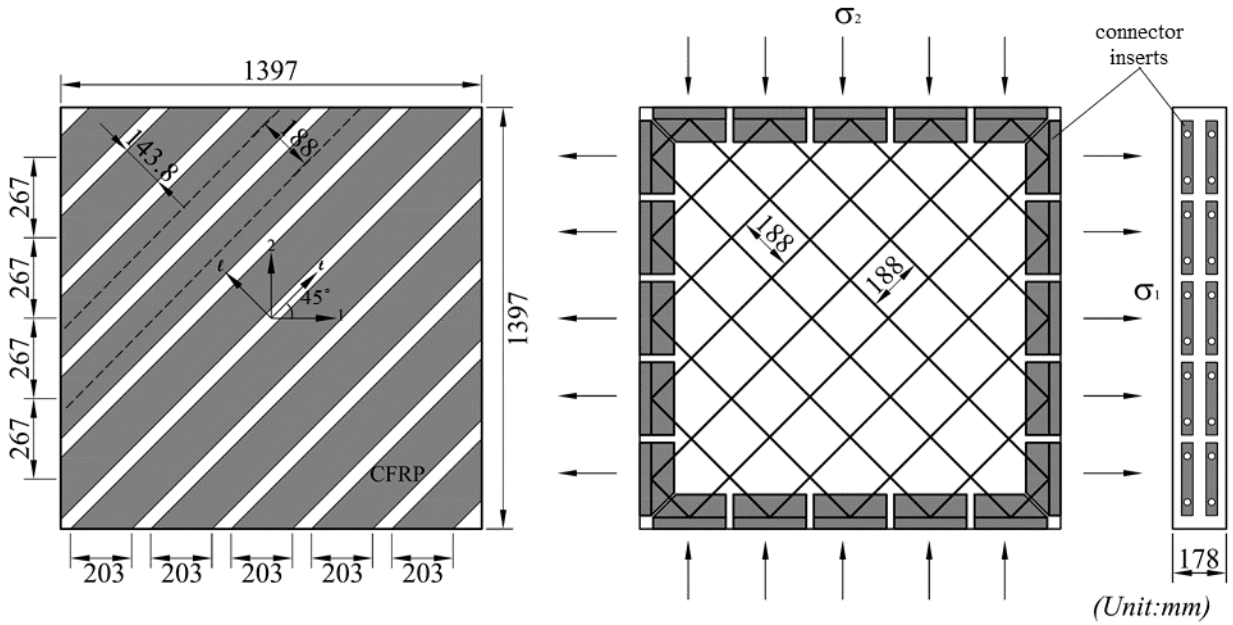

Fig. 1. Dimensions of test panels

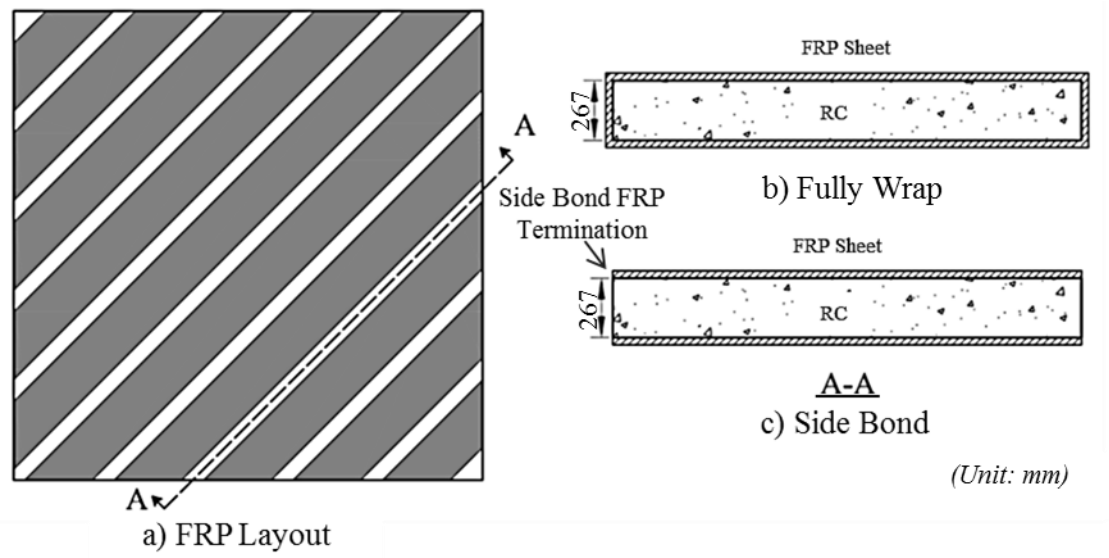

Fig. 2. Layout and wrapping method of FRP sheets, a) FRP layout, b) Fully wrap, and c) Side bond wrapping scheme cross sections

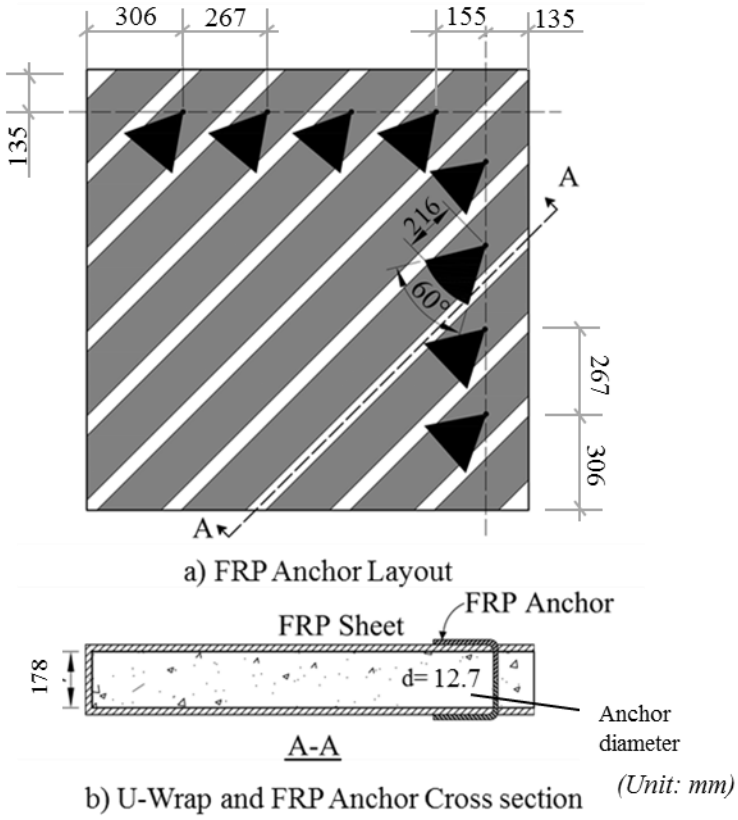

Fig. 3. U-Wrap with FRP anchor details

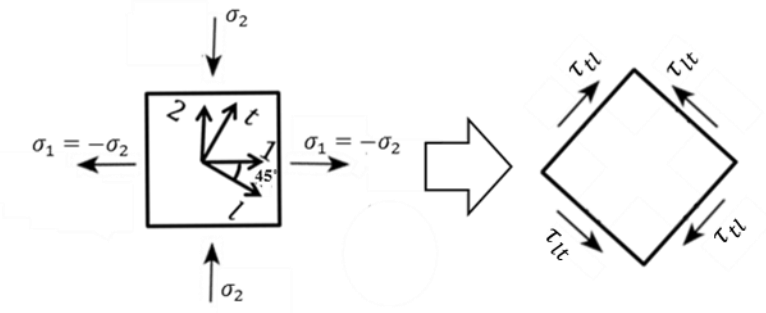

Fig. 4. Proportional loading of panel in 1-2 directions

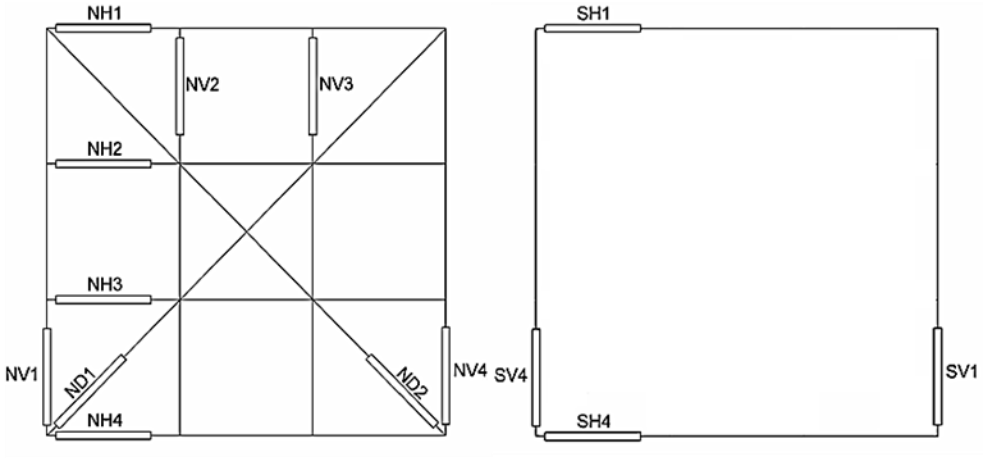

a) North Side b) South Side

Fig. 5. LVDT arrangement for the panel specimens

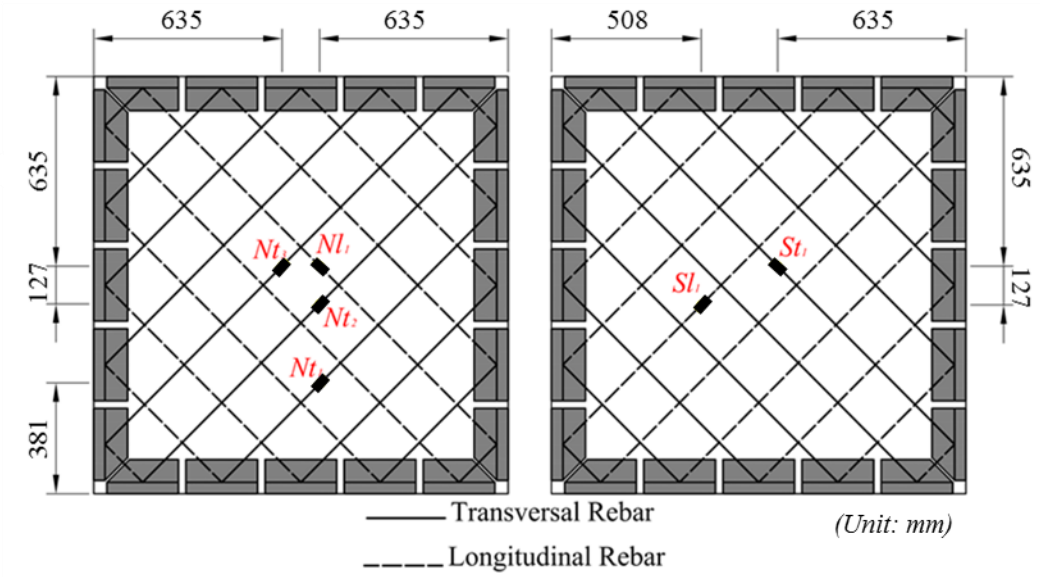

a) North Side b) South Side

Fig. 6. Strain gauge layout on steel rebar of panel specimens

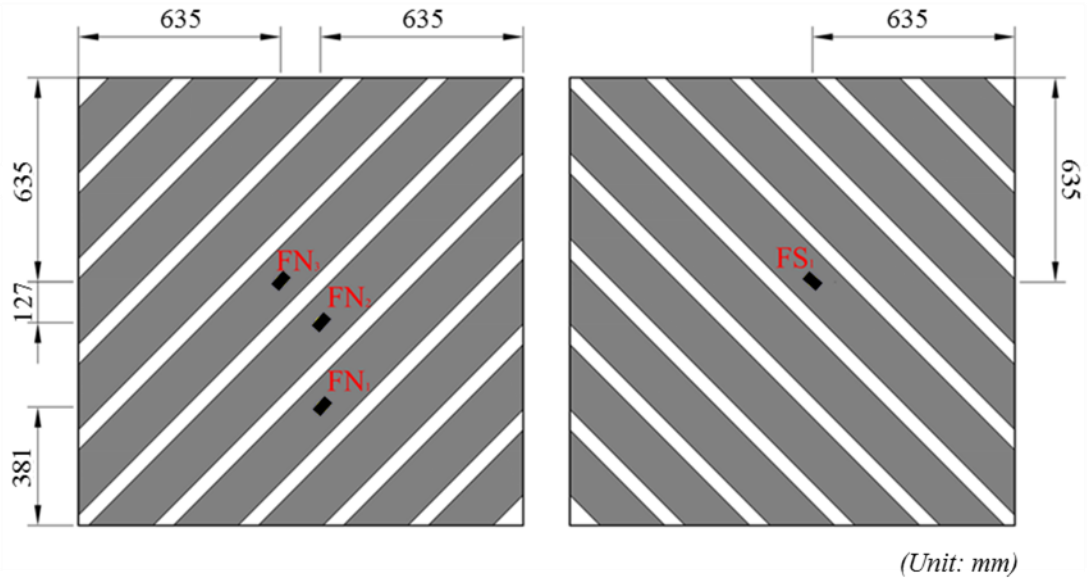

Fig. 7. Strain gauge layout on FRP sheets of panel specimens

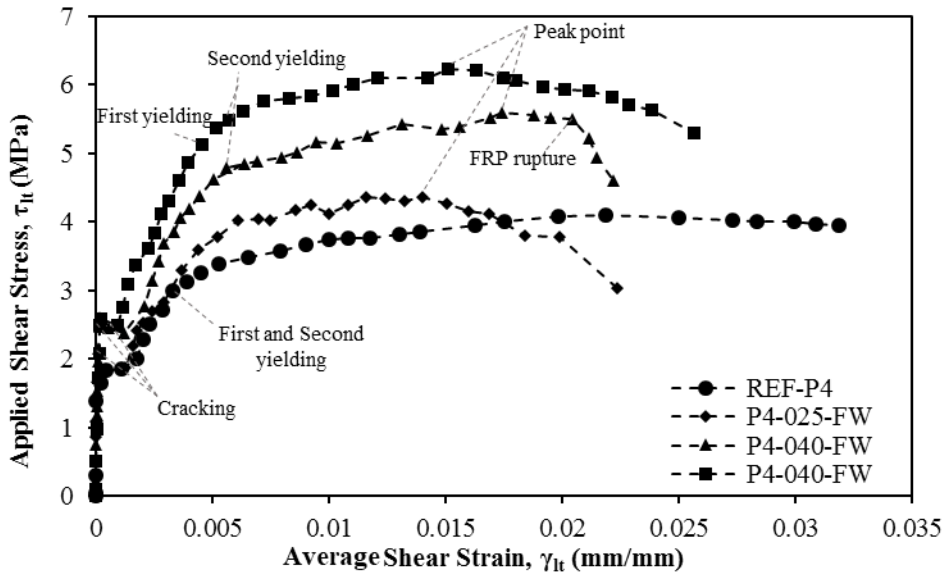

Fig. 8. Effect of FRP stiffness on shear stress-shear strain curves of panels P4-FW series

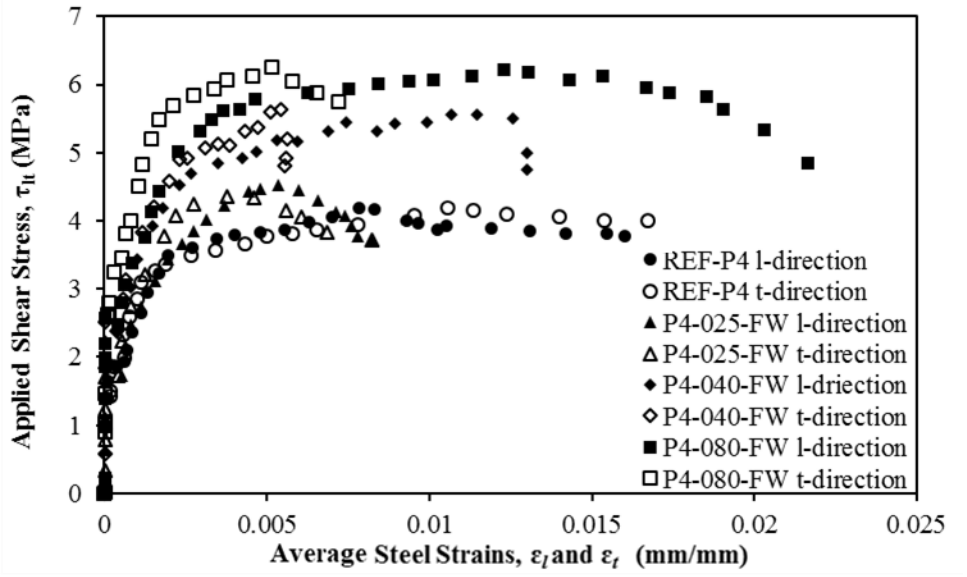

Fig. 9. Effect of FRP stiffness on $\tau_{lt} - \varepsilon_l$ and $\tau_{lt} - \varepsilon_t$ relationships of panels P4-FW series

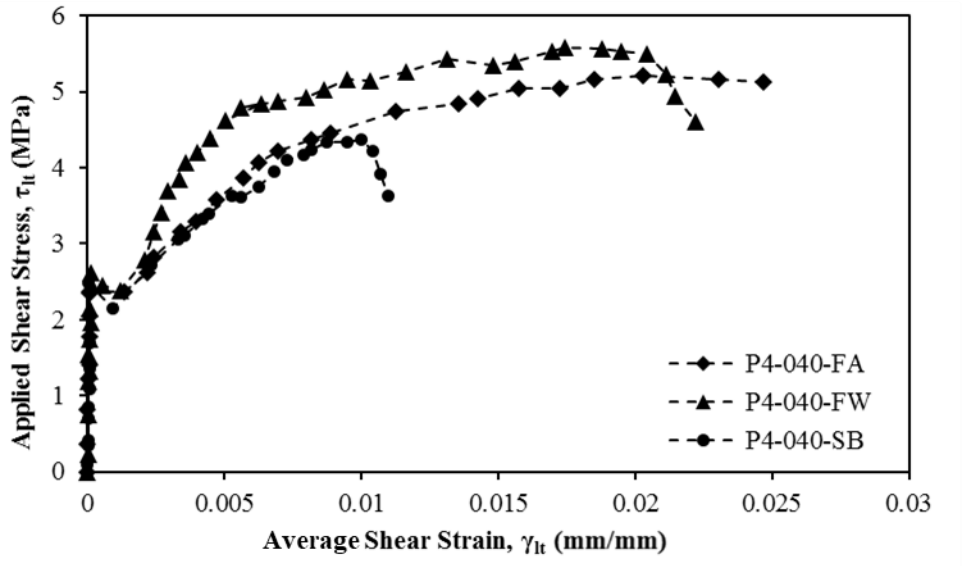

Fig. 10. Shear stress-strain curves for specimens with different wrapping schemes (panels P4-040 series)

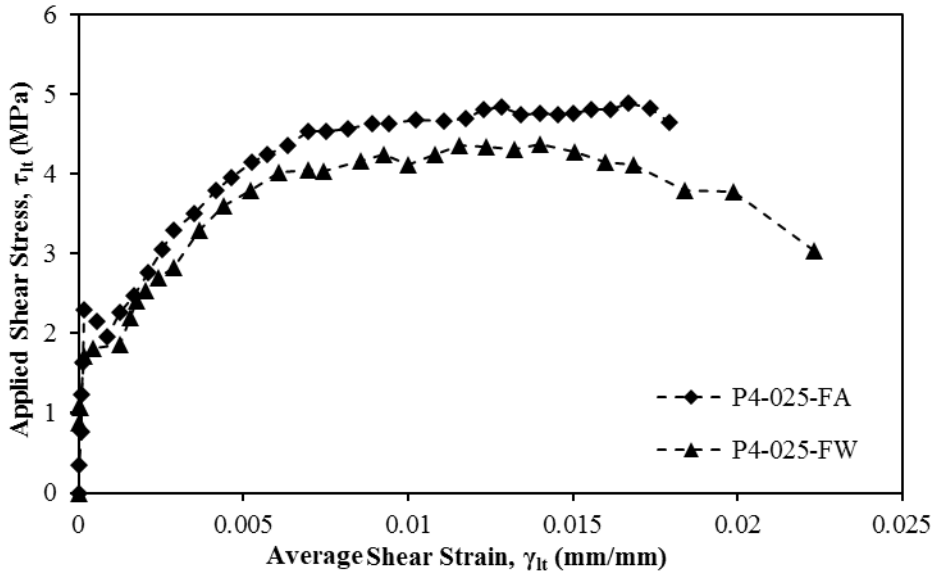

Fig. 11. Shear stress-strain comparison of wrapping scheme in panels P4-025 series

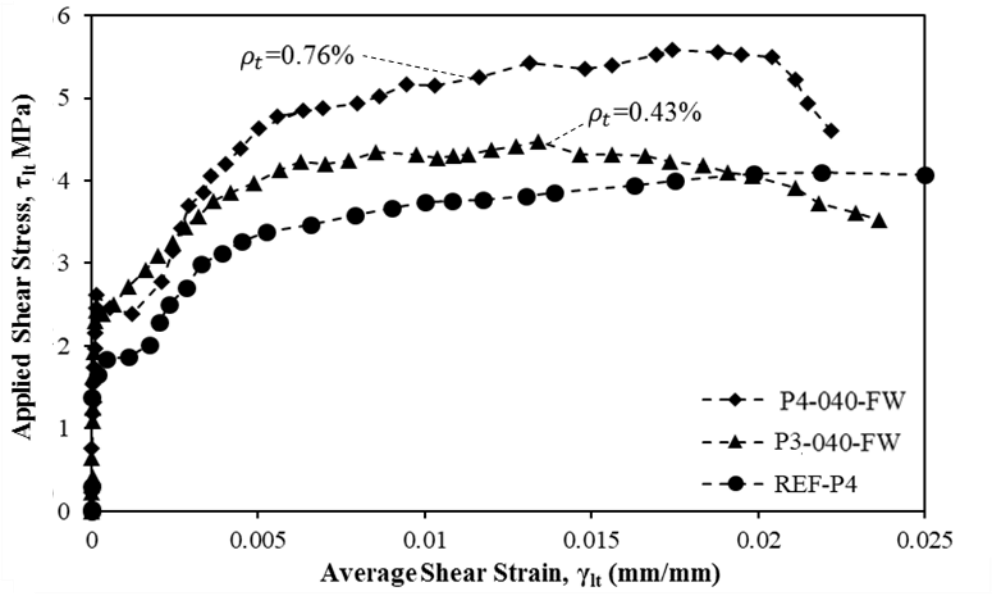

Fig. 12. Shear stress-strain comparison of transverse steel reinforcement in panels 040-FW series

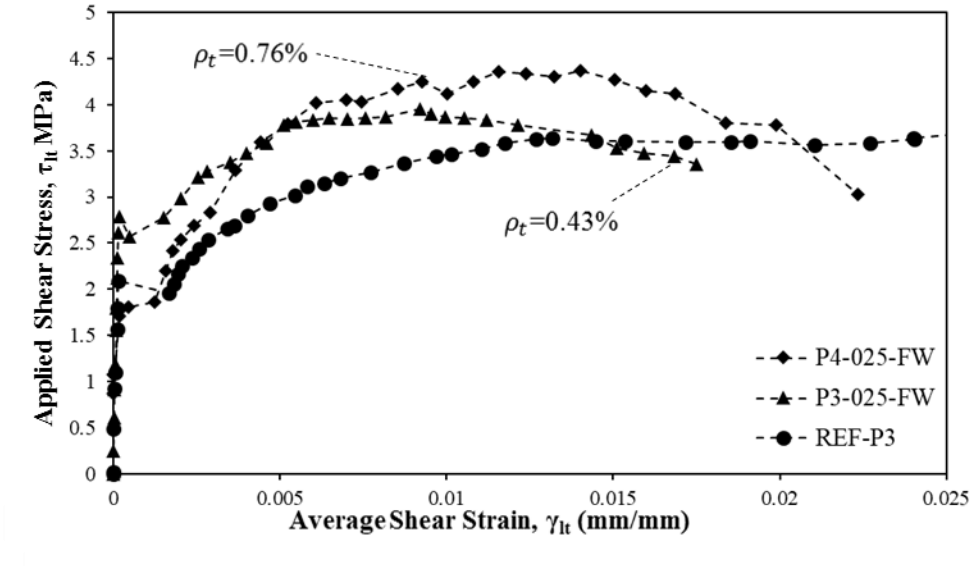

Fig.13. Shear stress-strain comparison of transverse steel reinforcement in panels 025-FW series

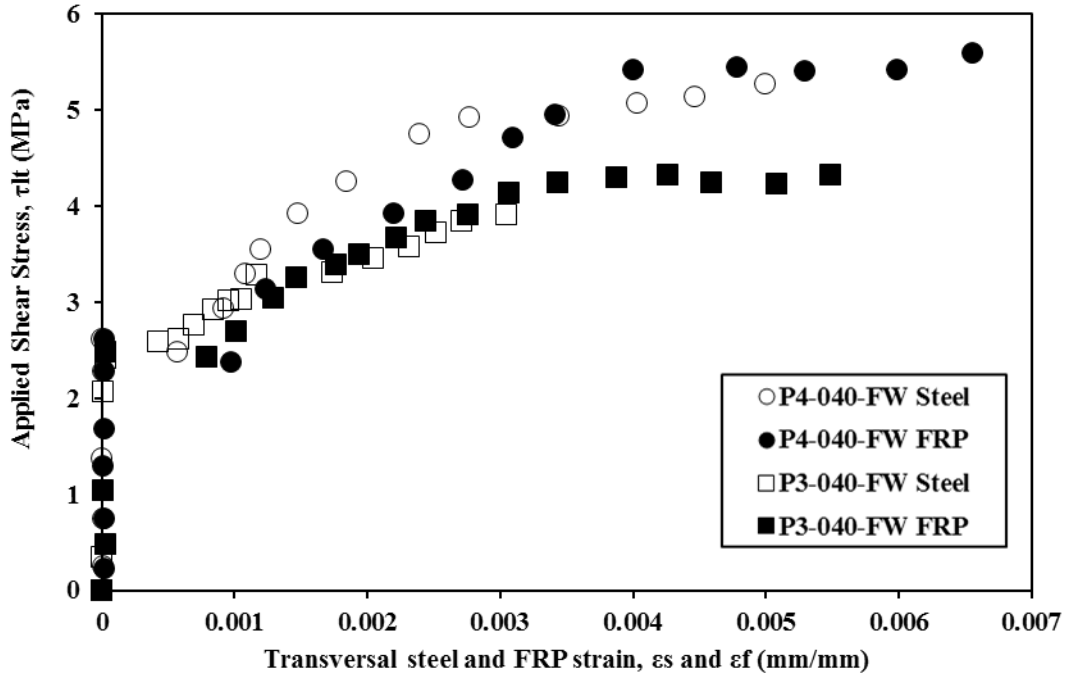

Fig. 14. Comparison of transverse steel strain and FRP of panels P4-040-FW and P3-040-FW

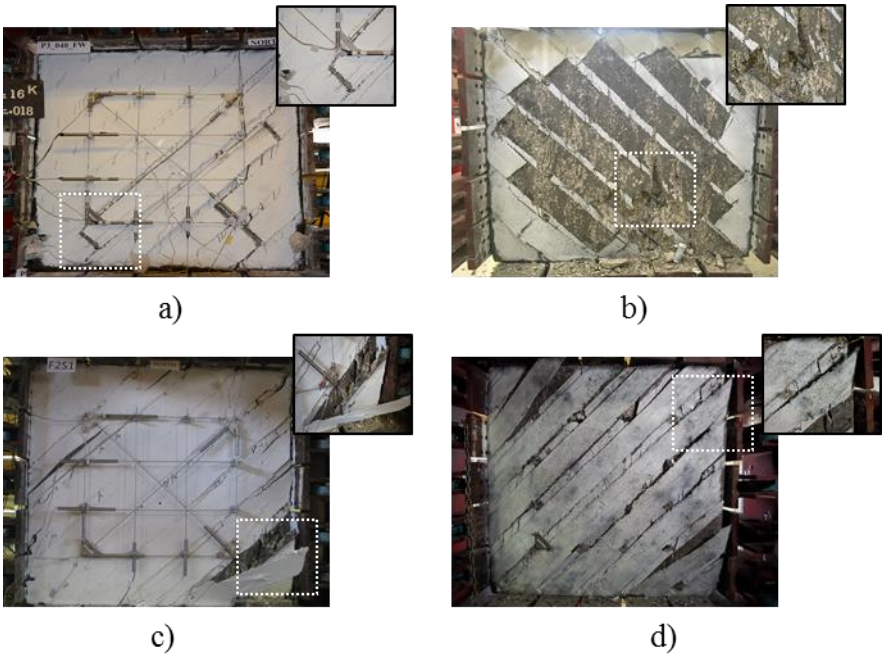

Fig. 15. Different failure modes of panel specimens, a) FRP debonding, b) Concrete crushing, c) FRP anchor failure, d) FRP rupture

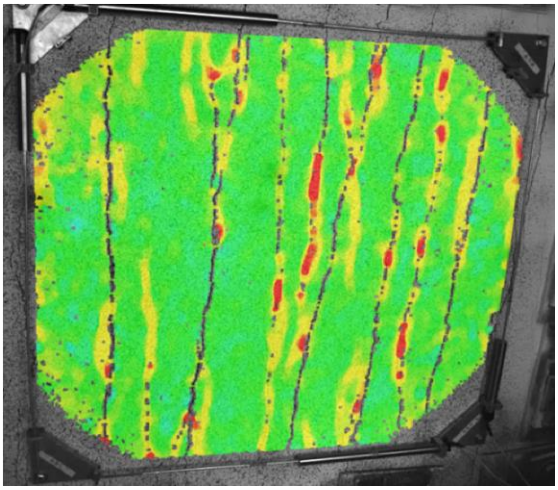

Fig. 16. Full strain field in the direction of applied load of specimen at a specific load level

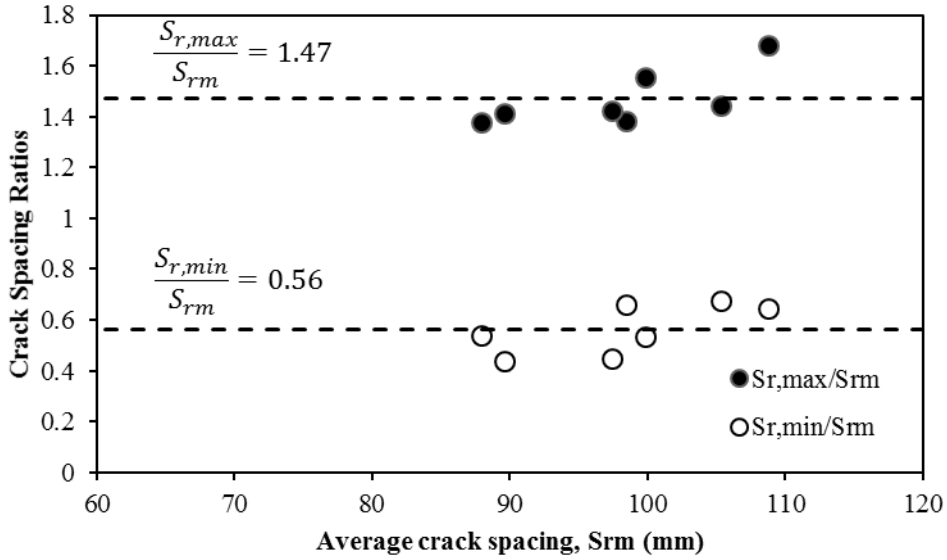

Fig. 17. Ratios of maximum and minimum to average crack spacing vs. average crack spacing in shear tests

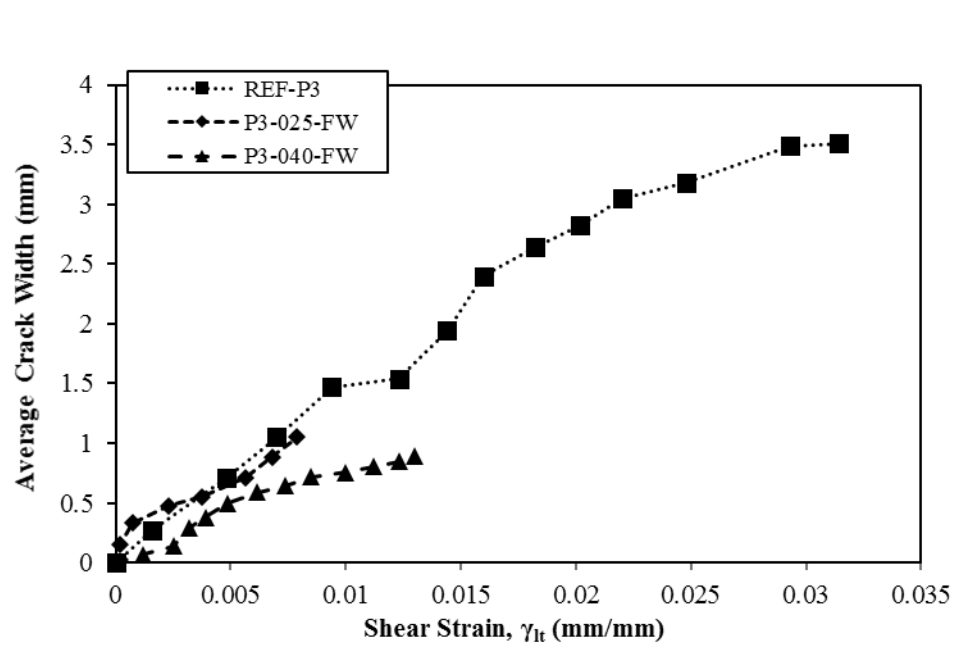

Fig. 18. Average crack width comparison of panel series P3-FW and REF-P3

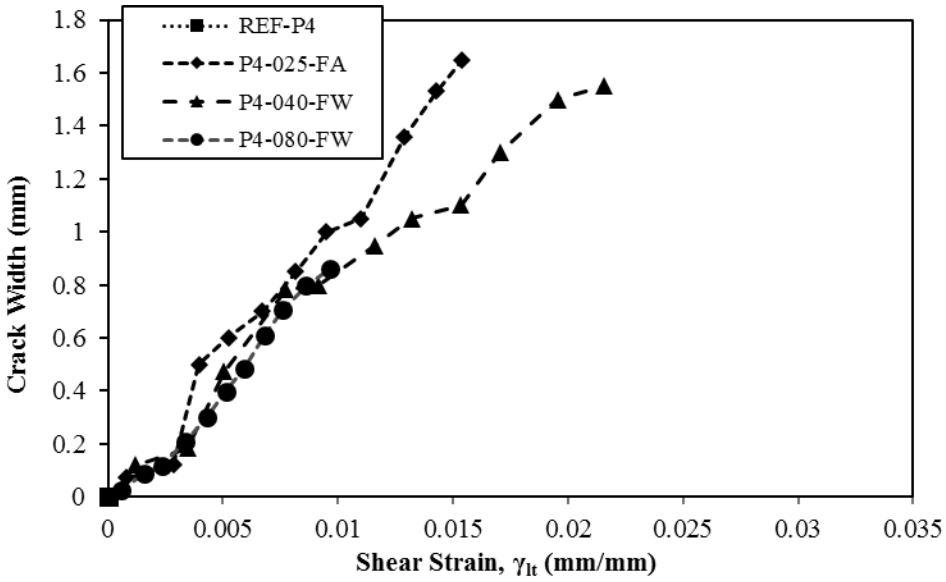

Fig. 19. Average crack width comparison of panel series P4-FW and P4-FA

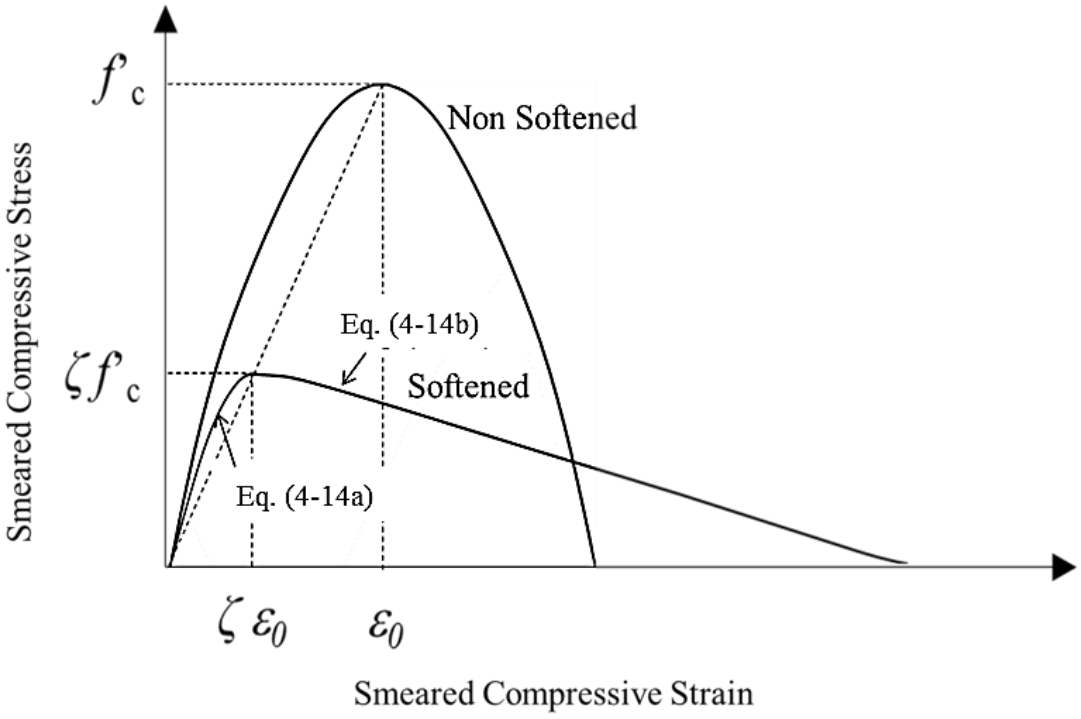

Fig. 20. Monotonic Non-Softened and Softened Stress-Strain Curve [15]

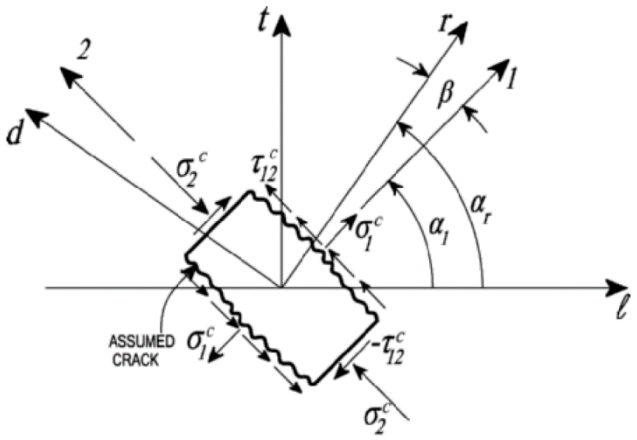

Fig. 21 Deviation Angle β [15]

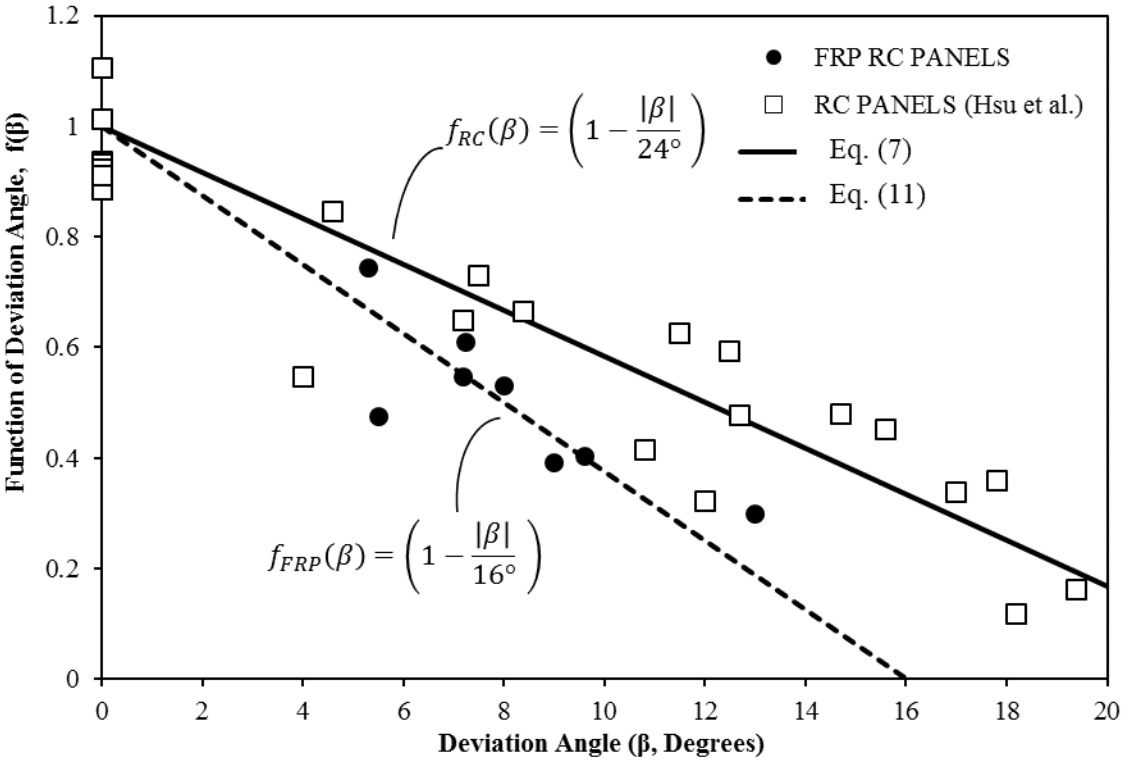

Fig. 22 $f(\beta)$ versus β Relationships for RC and FRP Strengthened RC Panels

Table 1. Principal variables of test panel and material properties

Series	Specimen Name	Concrete	Steel in *l* direction			Steel in *t* direction			FRP in *t* direction	
		f'_c (MPa)	ρ_l (%)	f_{ly} (MPa)	E_{ls} (MPa)	ρ_t (%)	f_{ty} (MPa)	E_{ts} (MPa)	ρ_f (%)	E_f (MPa)
REF	REF-P3	53	0.76	462	190000	0.43	459	188000	-	-
	REF-P4	52	0.76	462	190000	0.76	462	190000	-	-
P3-FW	P3-025-FW	51	0.76	462	190000	0.43	459	188000	0.54	82700
	P3-040-FW	50	0.76	462	190000	0.43	459	188000	0.87	72400
P4-FW	P4-025-FW	45	0.76	462	190000	0.76	462	190000	0.54	82700
	P4-040-FW	52	0.76	462	190000	0.76	462	190000	0.87	72400
	P4-080-FW	54	0.76	462	190000	0.76	462	190000	1.74	72400
P4-SB	P4-040-SB	44	0.76	462	190000	0.76	462	190000	0.87	72400
P4-FA	P4-025-FA	52	0.76	462	190000	0.76	462	190000	0.54	82700
	P4-040-FA	52	0.76	462	190000	0.76	462	190000	0.87	72400

Table 2. Applied stresses and corresponding measured strains at peak load stage

Series	Panel	σ_{2m} (MPa)	σ_{1m} (MPa)	τ_{ltm} (MPa)	ε_{20} (mm/mm)	ε_{10} (mm/mm)	ε_{l0} (mm/mm)	ε_{t0} (mm/mm)	γ_{lt0} (mm/mm)
REF	REF-P3	-3.6	3.3	3.5	-0.000113	0.0228	0.0073	0.0172	0.0229
	REF-P4	-4.1	4.1	4.1	-0.000147	0.0219	0.0085	0.0117	0.0220
P3-FW	P3-025-FW	-4.2	3.7	4.0	-0.000164	0.0108	0.00632	0.00429	0.1089
	P3-040-FW	-4.7	4.1	4.4	-0.000241	0.0121	0.0059	0.0060	0.0122
P4-FW	P4-025-FW	-4.0	4.4	4.2	-0.000265	0.0067	0.0037	0.0024	0.0070
	P4-040-FW	-5.5	5.6	5.6	-0.000798	0.0166	0.0100	0.0050	0.0174
	P4-080-FW	-6.6	5.9	6.3	-0.000328	0.0165	0.0177	0.0065	0.0162
P4-SB	P4-040-SB	-3.9	4.7	4.3	-0.000114	0.0089	0.0047	0.0018	0.0091
P4-FA	P4-025-FA	-5.1	4.8	4.9	-0.000233	0.0162	0.0098	0.0045	0.0164
	P4-040-FA	-5.6	5.0	5.3	-0.000101	0.0187	0.0131	0.0042	0.0188

Table 3. Failure modes of test specimens

Panel	REF-P3	REF-P4	P3-025-FW	P3-040-FW	P4-025-FW	P4-040-FW	P4-080-FW	P4-040-SB	P4-025-FA	P4-040-FA
Failure Mode	Concrete crushing	Concrete crushing	FRP rupture	FRP rupture	FRP rupture	FRP rupture	Concrete crushing	FRP debonding	Anchor Failure/rupture	FRP rupture

Table 4. Experimental maximum, minimum and average crack spacing of panels at stabilized cracking stage

Specimen	**No. of cracks**	**$S_{r,max}$ (mm)**	**$S_{r,min}$ (mm)**	**S_{rm} (mm)**
REF-P3	10	151.89	71.37	105.35
REF-P4	8	121.16	47.49	87.95
P3-0250-FW	12	182.82	70.38	108.81
P3-040-FW	11	136.14	65.02	98.46
P4-025-FA	10	138.94	43.44	97.43
P4-040-FW	12	154.94	53.16	99.79
P4-080-FW	13	126.49	39.37	89.57

Table 5. Calculation of β and $f(\beta)$ for FRP Strengthened RC Panels

Specimen	ζ_{exp}	$f_c^{'}$ (Mpa)	$f(f_c^{'})$	$\bar{\varepsilon}_1$	$f(\bar{\varepsilon}_1)$	$\rho_f E_f$ (Mpa)	$f(FRP)$	$f(\beta)_{exp}$	$\beta°$
P3-025-FW	0.184	51	0.812	0.017	0.367	463.3	1.164	0.529	8.0
P3-040-FW	0.158	50	0.820	0.012	0.413	651.6	1.193	0.390	9.0
P4-025-FW	0.198	45	0.864	0.012	0.415	463.3	1.164	0.473	5.5
P4-040-FW	0.204	52	0.804	0.018	0.349	651.6	1.193	0.608	7.3
P4-080-FW	0.110	54	0.789	0.016	0.367	1259.7	1.269	0.298	13.0
P4-040-SB	0.190	44	0.874	0.010	0.452	651.6	1.193	0.402	9.6
P4-025-FA	0.184	52	0.804	0.017	0.359	463.3	1.164	0.547	7.2
P4-040-FA	0.200	52	0.804	0.029	0.280	651.6	1.193	0.744	5.3